

Prediction of soil moisture scarcity using sequential Gaussian simulation in an arid region of China



Shuaipu Zhang^a, Mingan Shao^{a,b,*}, Danfeng Li^c

^a State Key Laboratory of Soil Erosion and Dryland Farming on the Loess Plateau, Northwest A&F University, Yangling 712100, Shaanxi, China

^b Key Laboratory of Ecosystem Network Observation and Modeling, Institute of Geographic Sciences and Natural Resources Research, Chinese Academy of Sciences, Beijing 100101, China

^c Key Laboratory of Water Cycle & Related Land Surface Processes, Institute of Geographic Sciences and Natural Resources Research, Chinese Academy of Sciences, Beijing 100101, China

ARTICLE INFO

Article history:

Received 25 September 2016

Accepted 5 February 2017

Available online 27 February 2017

Keywords:

Soil moisture scarcity

Spatial pattern

Risk analysis

Stochastic simulation

Uncertainty

ABSTRACT

Soil moisture plays a vital role in maintaining the sustainability of dryland ecosystems. Accurately predicting soil moisture scarcity (SMS) has an important interest of guidance to soil and water conservation. In this study, we gathered a time series of soil moisture measurements throughout the growing season (from April to October) in an area of approximately 100 km² in a desert oasis of northwestern China. Sequential Gaussian simulation was applied to investigate the spatial variability and scarcity of soil moisture across multiple land use types. Soil moisture exhibited considerable spatial heterogeneity with different magnitudes of spatial dependence at different times. Two hundred simulated realizations depicted the possible spatial variations of soil moisture in the geographic space. SMS was characterized as the natural event that occurred when the spatial probability of soil moisture not exceeding 0.15 cm³ cm⁻³ was greater than a critical threshold. With the increasing of probability thresholds, the proportion of SMS locations in each land use decreased at different rates. Given the spatial probability threshold of 0.6, 1.3–3.8% of the cultivated land, 2.6–5.2% of the forest land, 3.2–4.6% of the grassland, and 2.7–7.4% of the shrub land were of SMS during the measuring period. The newly cultivated land and the ecotone of desert and oasis were the major regions SMS occurred. Some soil moisture conservation measures such as precision irrigation should be taken to prevent the probable land degradation and agricultural disasters in these areas. The prediction of SMS using stochastic simulation contributes to improving soil water management in the oasis and provides a methodology reference for similar studies in risk analysis.

© 2017 Elsevier B.V. All rights reserved.

1. Introduction

Soil moisture is the major limiting factor for plant growth and plays an irreplaceable role in maintaining the sustainability of ecosystems in arid regions. A sensible policy of water resource management requires a thorough understanding of soil moisture variations. Accurately managing the variability of soil moisture has contributed greatly to numerous issues such as constructing farmland shelterbelts (Wang et al., 2008; Yan et al., 2015), preventing land degradation (Berndtsson et al., 1996; Kairis et al., 2014), and improving irrigation efficiency (Chang et al., 2015; Stabler, 2008). The actual procedure of soil and water conservation practice depends upon the clear recognition of soil moisture scarcity (SMS). To prevent ecological and agricultural damage in a timely manner, adopting a technical and scientific approach is essential to successfully forecast the dynamics of soil moisture and assess the risk of SMS (Deng et al., 2011; Srivastava et al., 2013).

Soil moisture dynamics are controlled by a range of geophysical parameters in the field (e.g. topography, soil properties, vegetation density, and regional climate) (Li et al., 2016; She et al., 2014). The estimation of soil moisture at any unsampled location using a limited number of sample measurements has the property to involve some degree of uncertainty (Castrignanò and Buttafuoco, 2004). Encouragingly, geostatistics based on Kriging and simulation provides effective approaches to predict the spatial distribution of soil properties. In recent decades, stochastic simulation algorithms have been increasingly used to field studies (Pachepsky and Acock, 1998; Pardo-Iguzquiza and Chica-Olmo, 2008; Van Meirvenne and Goovaerts, 2001; Yao et al., 2013), especially in the situation where the spatial variation of the measured field must be preserved (Goovaerts, 1999). This technique can avoid the smoothing effects of Kriging estimators (Deutsch and Journel, 1998) and provide more reliable simulated results through computing plenty of possible realizations of the unknown spatial distribution (Delbari et al., 2009; Leuangthong et al., 2004). Not only that, the uncertainty of estimation for the soil property in question at unsampled locations can be assessed with probability modeling through post-processing of the set of alternative realizations, which offers new opportunities for risk evaluation (Goovaerts, 1997). Thus, quantizing the

* Corresponding author.

E-mail address: mashao@ms.iswc.ac.cn (M. Shao).

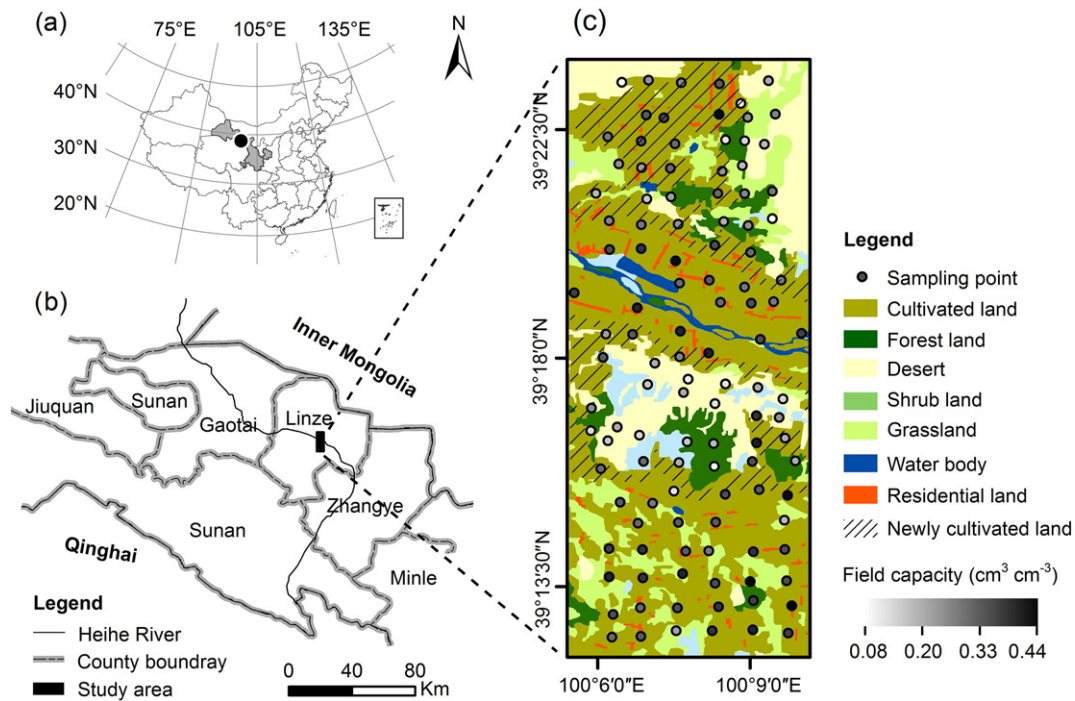


Fig. 1. Location of the study area in Gansu Province of China (a) and Linze County (b), and field capacities of the sampling points on the land use map (c).

uncertainty of soil moisture using conditional stochastic simulation makes it possible to predict SMS. The feasibility of applying this method to the prediction of soil moisture has been confirmed in previous reports (Bourennane et al., 2007; Castrignanò and Buttafuoco, 2004). Some researchers satisfactorily delineated soil vulnerability to erosion by assessing the uncertainty of soil moisture in a few areas (Afrasiab and Delbari, 2013; Delbari et al., 2009). Actually, there are not many applications of geostatistical simulation in risk analysis of SMS in soil water management. The current study, therefore, attempted to predict SMS using stochastic simulation and then expand the output to actual practice. This may improve the utility of soil water management and offer a reference for decision-making.

We gathered a time series of soil moisture measurements throughout the growing season in an oasis area of northwestern China. The spatial patterns of soil moisture were investigated with sequential Gaussian simulation (SGS), one of the most proposed simulation algorithms for continuous variables. SMS was defined as the natural event that occurred when the spatial probability of soil moisture content not exceeding 60% of the field capacity was greater than a critical probability threshold. The primary objectives of this study were: i) to reveal the spatial variations of soil moisture at different times, ii) to predict SMS and explore its seasonal activities.

2. Materials and methods

2.1. Study area

The study was conducted in an area of approximately 100 km² (100°05'32"–100°10'01"E, 39°12'35"–39°23'28"N) in Linze County, Gansu Province, China (Fig. 1). Linze County is in the middle reaches of the Heihe River and within a representative piedmont plain. This area has a typical continental arid climate with strong solar radiation, low precipitation, and high evaporation. The mean annual precipitation is 117 mm for many years, approximately 65% of which falls between July and September. The mean annual pan evaporation is around 2365 mm. The mean annual air temperature is 7.6 °C, with minimum and maximum temperatures of −27.8 °C in January and 39.1 °C in July, respectively. The regional soil is grey-brown desert soil with eolian sand on the margins of the oasis (Liu et al., 2010). The growing season is from May to October, and the frost-free period is about 165 days (Zhao and Liu, 2010).

The Heihe River originates in the Qilian Mountains and supplies most of the water for the oasis ecosystem. The land use types of the study area are diverse, mainly including cultivated land, forest land, shrub land, grassland, and desert (Fig. 1c) (10.3972/heihe.100.2014.

Table 1

The basic information of soil properties and vegetation composition in each land use.

Land use	Clay (<0.002 mm) (%)	Silt (0.002–0.05 mm) (%)	Sand (>0.05 mm) (%)	Bulk density (g/cm ³)	Vegetation
Cultivated land	27.71	39.01	33.24	1.49	Wheat (<i>Triticum aestivum</i> Linn.), maize (<i>Zea mays</i> Linn.), cotton (<i>Gossypium hirsutum</i> Linn.), etc.
Forest land	17.22	21.10	61.43	1.53	Poplar (<i>Populus gansuensis</i> C. Wang et H. L. Yang), elm (<i>Ulmus pumila</i> L.), sand jujube (<i>Elaeagnus angustifolia</i> Linn.), etc.
Shrub land	11.95	15.49	72.34	1.55	<i>Haloxylon ammodendron</i> (C. A. Mey.) Bunge, <i>Tamarix chinensis</i> Lour., <i>Calligonum arborescens</i> Litv., etc.
Grassland	26.69	40.21	32.85	1.50	<i>Setaria viridis</i> (L.) Beauv., <i>Phragmites australis</i> (Cav.) Trin. ex Steud., <i>Leymus secalinus</i> (Georgi) Tzvel., <i>Agropyron cristatum</i> (L.) Gaertn., etc.
Desert	5.39	6.21	88.08	1.65	<i>Halogeton arachnoideus</i> Moq., <i>Bassia dasyphylla</i> (Fisch. et Mey.) O. Kuntze, <i>Salsola passerina</i> Bunge, etc.

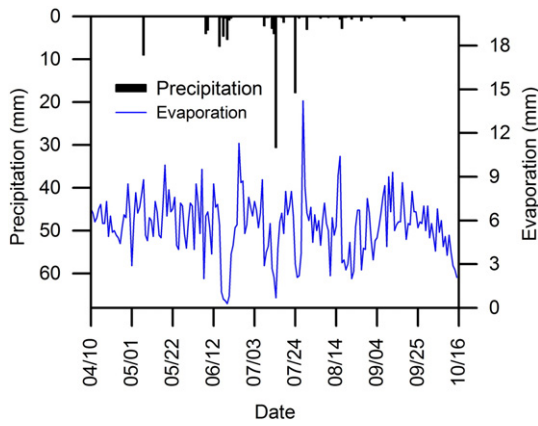


Fig. 2. Daily precipitation and evaporation through the measurement period.

db). Most of the available lands bordering the desert are newly cultivated. Table 1 shows the basic information of soil properties and vegetation composition for each land use. The cultivated lands are irrigated with water from the Heihe River as well as the groundwater.

2.2. Soil moisture measurements

A grid sampling scheme was adopted for a good coverage over the study area (Fig. 1c). The rectangular space (20 × 5 km) was sectioned into a grid of 1 × 1 km squares, and 126 sampling points were initially determined. Eleven of these points, however, were absent due to the occurrence of roads, buildings, reservoirs, and river channels. An aluminum neutron-probe access tube was installed at each location. Soil moisture was measured at the depth of 0–100 cm using a neutron probe. Neutron counts were recorded at depth increments of 10 cm and then were converted to volumetric soil moisture contents with a calibration curve. Taking into account the escape of neutrons from the surface soil (Chanasyk and Naeth, 1988; Evett et al., 2003), 0–20 cm was treated differently from 20–100 cm when doing the calibration of neutron probe. The depth-specific calibration has been proven to be highly valid for the profile by Li (2014). The volumetric soil moisture content at location *i* and depth *j*, $w_{i,j}$ ($\text{cm}^3 \text{cm}^{-3}$), was calculated by:

$$w_{i,j(0-20 \text{ cm})} = 0.978CR_{i,j} - 0.033 \quad (R^2 = 0.89, p < 0.001) \quad (1)$$

$$w_{i,j(20-100 \text{ cm})} = 0.690CR_{i,j} - 0.031 \quad (R^2 = 0.92, p < 0.001) \quad (2)$$

where *CR* is slow-neutron counting rate, i.e., the ratio of recorded to standard count.

The monitoring of soil moisture was carried out in the middle of each month from April to October in 2013, a normal year in meteorology. Fig. 2 shows the daily precipitation and evaporation through the measurement period.

Table 2
Descriptive statistics of soil moisture measurements ($\text{cm}^3 \text{cm}^{-3}$) throughout the growing season.

Month	Minimum	Maximum	Mean	SD ^a	CV	Kurtosis	Skewness	K–S ^b
April	0.01	0.55	0.16	0.14	0.85	–0.45	0.64	N
May	0.01	0.53	0.15	0.13	0.84	–0.66	0.58	N
June	0.01	0.41	0.15	0.12	0.81	–1.17	0.40	N
July	0.02	0.53	0.17	0.12	0.72	–0.51	0.50	N
August	0.01	0.47	0.17	0.13	0.77	–1.13	0.37	N
September	0.02	0.49	0.17	0.13	0.76	–1.20	0.36	N
October	0.01	0.47	0.16	0.12	0.77	–0.96	0.52	N

^a SD, standard deviation; CV, coefficient of variation.

^b The significance level of K–S test is 0.05. The capital letter N indicates that the data is not in Gaussian distribution.

2.3. Sequential Gaussian simulation

Sequential Gaussian simulation can be characterized as simulating Gaussian random functions using sequential simulation algorithm. Based on the multi-Gaussian assumption of a random function model, SGS randomly draws a simulated value at each location from an estimated conditional cumulative distribution function (ccdf). The ccdf is determined by the kriging mean and variance computed from the neighborhood information. When running the SGS, a prior transform of the original data into a Gaussian distribution is necessary and can be normally performed by the normal score transformation (Goovaerts, 1997; Remy et al., 2009).

For a Gaussian continuous variable $Z(\mathbf{u})$, the experimental semivariogram $\gamma(\mathbf{h})$ is calculated by:

$$\gamma(\mathbf{h}) = \frac{1}{2N(\mathbf{h})} \sum_{i=1}^{N(\mathbf{h})} [z(\mathbf{u}_i) - z(\mathbf{u}_{i+h})]^2 \quad (3)$$

where $N(\mathbf{h})$ is the number of data pairs separated by distance \mathbf{h} , $z(\mathbf{u}_i)$ and $z(\mathbf{u}_{i+h})$ are the sample values for $Z(\mathbf{u})$ at location \mathbf{u}_i and \mathbf{u}_{i+h} , respectively. The best fitted theoretical function model can be determined using cross validation. Generally, the model is described by the parameters of nugget value (C_0), structural variance (C), sill ($C_0 + C$), and range (A). The nugget coefficient ($C_0 / (C_0 + C)$) indicates the degree of spatial dependence that can be divided into three levels: <0.25, strong; 0.25–0.75, medium; >0.75, weak (Cambardella et al., 1994).

Based on the semivariogram model, the SGS algorithm can be detailed by the following procedure (Remy et al., 2009):

- 1) Determine a random path through the grid nodes.
- 2) At each node \mathbf{u} , do the following:
 - Define a search ellipsoid to obtain conditional information (raw data and previously simulated values).
 - Estimate the mean and variance of the local ccdf as a Gaussian distribution using Kriging with the semivariogram model, $\gamma(\mathbf{h})$.
 - Draw a random value from the ccdf and add the simulated value to the data set.
- 3) Repeat this process until all nodes are simulated.

Repeating these sequential steps with different random paths can provide multiple realizations of the spatial distribution of $Z(\mathbf{u})$ in the space of interest. In this study, to get a precise and accurate probability calculation, the SGS algorithm was conducted two hundred times in the Stanford Geostatistical Modeling Software (SGeMS) package.

2.4. Uncertainty of soil moisture

The simulations of soil moisture have the same probability of occurrence then the whole set of simulations gives a measure of uncertainty. The uncertainty of soil moisture at any unsampled location can be assessed by probabilistic calculation (Delbari et al., 2009; Goovaerts, 2001). Suppose there are L amount of simulated realizations. The probability of soil moisture $z(\mathbf{u})$ not exceeding a critical threshold z_t at the

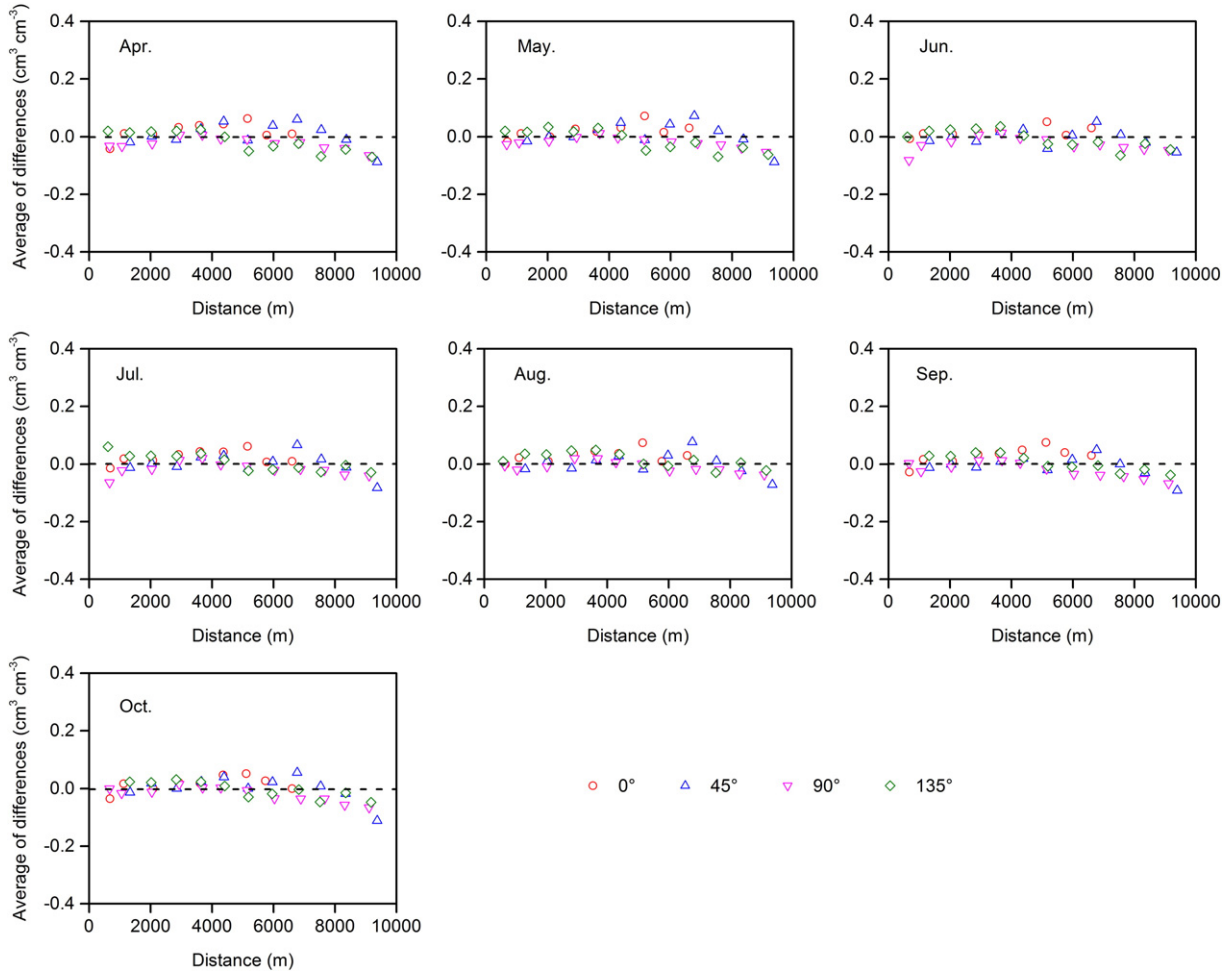


Fig. 3. The average of differences in soil moisture content at each lag distance in different directions.

location \mathbf{u} , i.e., $\text{Prob}[z(\mathbf{u}) \leq z_t]$, is calculated by the following equation:

$$\text{Prob}[z(\mathbf{u}) \leq z_t | (n)] = \frac{1}{L} \sum_{l=1}^L i^{(l)}(\mathbf{u}, z_t) \quad (4)$$

where $|(n)$ expresses conditioning to the local information (n point data). The indicator value $i^{(l)}(\mathbf{u}, z_t)$ is 1 if the simulated z -value does not exceed z_t , and 0 otherwise. With this equation, a probability map can be drawn to visualize the possibility of soil moisture being less than z_t .

For applications such as soil water management, it would make more sense to measure the joint probability about soil moisture status at several locations taken together than to measure the individual probability at a single location. Given a critical threshold of individual probability P_i , a specific area consisting of J amount of locations can be determined from the probability map by the provision $\text{Prob}[z(\mathbf{u}) \leq z_t] > P_i$. The spatial probability that soil moisture contents at the J locations are jointly not great than z_t can be calculated by:

$$\text{Prob}[z(\mathbf{u}_j) \leq z_t, j = 1, \dots, J | (n)] = \frac{1}{L} \sum_{l=1}^L \prod_{j=1}^J i^{(l)}(\mathbf{u}_j, z_t) \quad (5)$$

where L is the total number of realizations, and $i^{(l)}(\mathbf{u}_j, z_t)$ is 1 if $z^{(l)}(\mathbf{u}_j) \leq z_t$, and 0 otherwise.

2.5. Soil moisture scarcity

The critical threshold of soil moisture z_t was given as $0.15 \text{ cm}^3 \text{ cm}^{-3}$ corresponding for the study area to 60% of the mean field capacity. 60% field capacity has often been regarded as the lower limit of soil moisture content in irrigation management (Lamm and Rogers, 2015; Zhang et al., 2008). The field capacity (Fig. 1c) was measured using Wilcox method with the undisturbed soil samples collected by cutting ring (Duan et al., 2010; Hanks et al., 1954).

Soil moisture scarcity can be considered as a natural risk event at a time. We defined that if the spatial probability of soil moisture not exceeding the threshold of $0.15 \text{ cm}^3 \text{ cm}^{-3}$ was higher than a critical threshold P_s , there was an occurrence of SMS in the study area. The risk of SMS was analyzed under a range of probability thresholds ($0.5 \leq P_s \leq 0.95$).

3. Results

3.1. Exploratory data analysis

Table 2 shows the descriptive statistics of soil moisture for each month. The mean soil moisture varied slightly from 0.15 to $0.17 \text{ cm}^3 \text{ cm}^{-3}$ throughout the growing season. The maximum and minimum ranges were 0.01 – $0.55 \text{ cm}^3 \text{ cm}^{-3}$ in April and 0.01 – $0.41 \text{ cm}^3 \text{ cm}^{-3}$ in June, respectively. Soil moisture was typically characterized by high spatial heterogeneity over the study area, indicated by the coefficients of variation (CVs) varying between 0.72 and 0.85 .

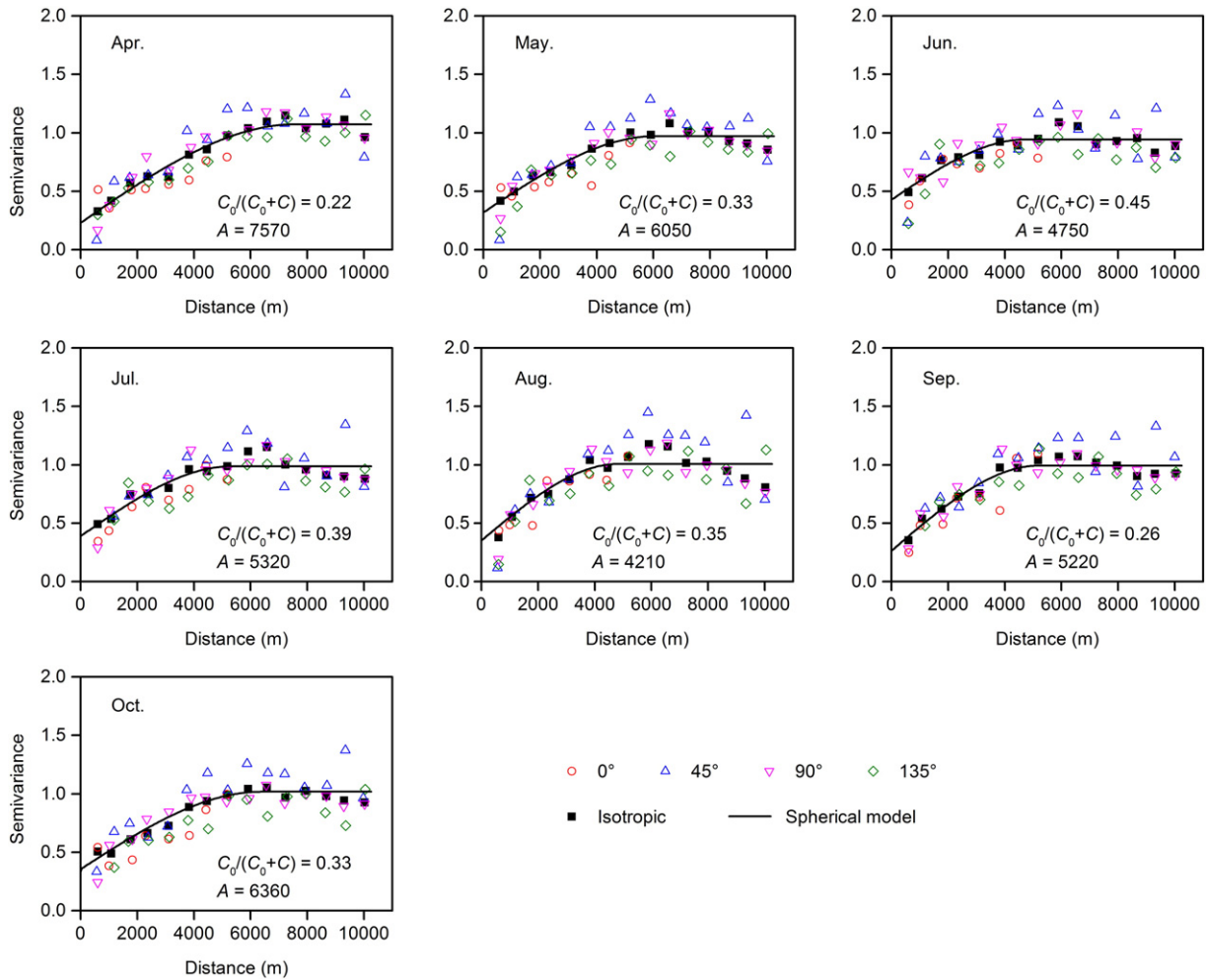


Fig. 4. Anisotropic and isotropic semivariograms of normal score transformed data. The bested fitted model of isotropic semivariogram for each set of data is spherical (solid line).

The spatial variability was higher in spring (April and May) than in summer (June, July, and August) and autumn (September and October).

As Gaussian simulation algorithm requires a multi-Gaussian framework, the normality of soil moisture values was examined by Kolmogorov–Smirnov test. All the data sets were positively skewed and did not follow normal distribution ($p < 0.05$) (Table 2). Thus, the raw data were transformed into Gaussian variables using a normal score transformation (Deutsch and Journel, 1998) and assuming a multi-normal distribution. The simulation results were back-transformed afterwards. Moreover, we calculated the differences in soil moisture contents between any two locations within about half the sampling extent. The average of the differences at each lag distance for different directions (0, 45, 90 and 135°) is presented in Fig. 3. No

significant spatial trends existed and the statistic features are deemed to be not against the second order stationary assumption.

3.2. Stochastic simulations of soil moisture

Anisotropic semivariograms of soil moisture were calculated in the directions of 0, 45, 90 and 135° with an angular tolerance of $\pm 22.5^\circ$. There were no significant directional behaviors, as evidenced by mild discrepancies resulting from the small number of data pairs. Therefore, the isotropic semivariograms were computed and fitted by the commonly used geostatistical models (spherical, exponential, and Gaussian) (Fig. 4). Cross validation showed that the spherical model was optimal for all the data sets. Soil moisture had different degrees of spatial dependence at different times. All the nugget coefficients were between 0.25 and 0.75 except April, suggesting that the spatial dependence was medium from May to October. The nugget coefficient of 0.22 indicated a strong spatial dependence in April. The ranges of soil moisture varied between 4210 and 7570 m during the study period. Summer had higher nugget coefficients and smaller ranges than spring and autumn.

Two hundred realizations of soil moisture spatial patterns were generated each month on a 50×50 m grid using SGS. The performances of nodal simulation relied on the simple Kriging estimator. The realization number was determined in the light of the overall error variances of simulated data, which tended to be constant after performing the algorithm 50 times. Table 3 shows the summary statistical characteristics over the whole data set of simulations. Compared with the observed

Table 3
Summary statistics over the whole simulated realizations of soil moisture ($\text{cm}^3 \text{cm}^{-3}$).

Month	Minimum	Maximum	Mean	SD ^a	CV
April	0.01	0.55	0.16	0.13	0.81
May	0.01	0.53	0.15	0.12	0.80
June	0.01	0.41	0.15	0.11	0.73
July	0.02	0.53	0.17	0.11	0.65
August	0.01	0.47	0.17	0.12	0.71
September	0.02	0.49	0.17	0.12	0.71
October	0.01	0.47	0.15	0.11	0.73

^a SD, standard deviation; CV, coefficient of variation.

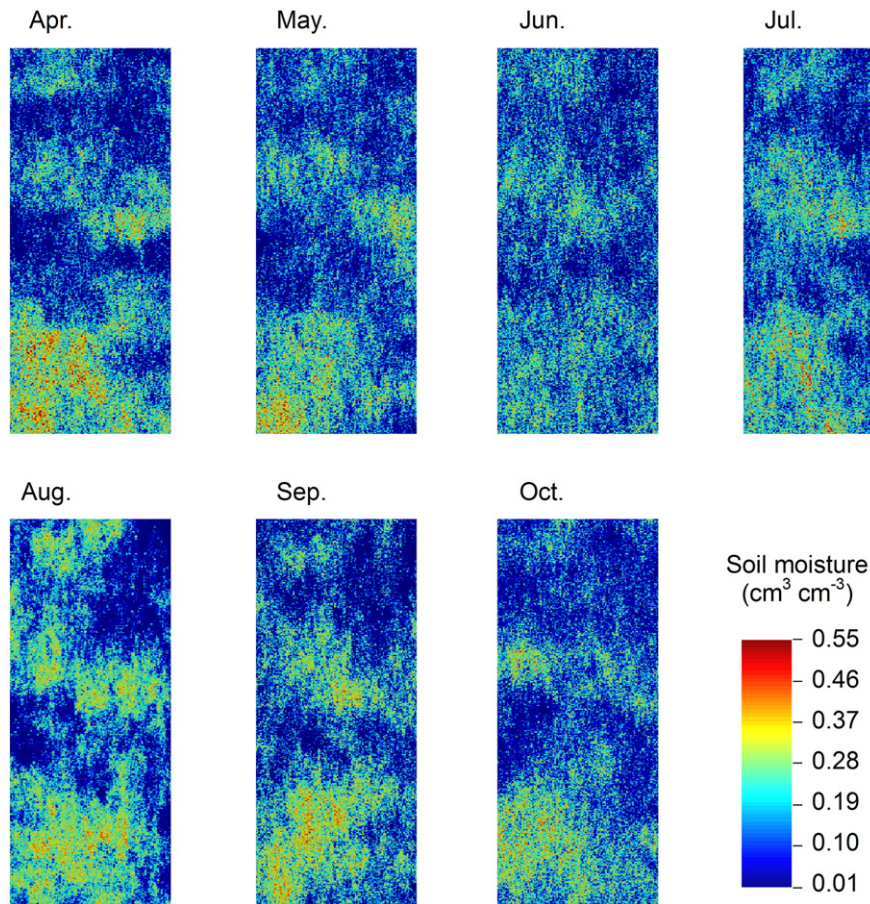


Fig. 5. Possible spatial distributions of soil moisture using sequential Gaussian simulation. One randomly selected realization is presented for each month.

data (Table 2), the simulated results had nearly identical means (0.15 to $0.17 \text{ cm}^3 \text{ cm}^{-3}$) and relatively lower CVs (0.65 to 0.81). Levene's test was carried out at the 0.05 level of significance to examine the homogeneity of variance between the two distributions for the monthly data. No heteroscedasticity was detected.

The set of individual realizations provided exhaustive descriptions of the spatial distribution of soil moisture over the study area. Fig. 5 shows one randomly selected realization for each month. Averaging all the realizations provided the expected estimates of soil moisture, i.e., the E-type values. The time series of E-type maps depicted the overall spatial patterns of soil moisture (Fig. 6).

3.3. Prediction of soil moisture scarcity

With the given threshold of $0.15 \text{ cm}^3 \text{ cm}^{-3}$, the uncertainty of soil moisture was expressed by $\text{Prob}[z(\mathbf{u}) \leq 0.15 \text{ cm}^3 \text{ cm}^{-3}]$ at any particular location based on the post-processing of SGS. The probabilities of soil moisture not exceeding $0.15 \text{ cm}^3 \text{ cm}^{-3}$ were mapped (Fig. 7). High probability values focused on the northeastern and south-central parts of the study area, corresponding to the low soil moisture locations in the E-type maps (Fig. 6).

According to the definition of SMS, soil moisture was of scarcity at locations where the spatial probability was higher than a critical probability threshold P_s . Fig. 8 shows the proportion of SMS grid units in each land use under different P_s values. Desert was abandoned due to the lack of vegetation. The proportion of SMS locations gradually declined with the increasing of P_s . Taking $P_s = 0.6$ as an example, SMS locations occupied 3.8%, 4.1%, 3.0%, 2.2%, 3.4%, 3.3% and 5.2% of the entire study area from April to October, respectively. The ranges of SMS percentages in cultivated land, forest land, grassland, and shrub land throughout the

growing season were 1.3–3.8%, 2.6–5.2%, 3.2–4.6%, and 2.7–7.4%, respectively.

4. Discussion

4.1. Spatial distribution of soil moisture

Driven by the complex interaction of local controls such as soil, vegetation, and irrigation and nonlocal controls such as climate and runoff (Vereecken et al., 2014), soil moisture exhibited great heterogeneity with medium or strong spatial dependence in the geographic space. Semivariogram analysis showed that the spatial dependence of soil moisture was higher in spring and autumn than in summer. The result was mainly because irregular rainfall, high evapotranspiration, frequent watering and grazing enhanced the random variations from June to August. The seasonal changes of spatial organization were also observed by Hu et al. (2011) for the land surface soil moisture in a semiarid area. They found a positive relationship between the magnitude of spatial dependency and soil moisture status. But in this study, there was a lack of significant correlation between the mean soil moisture and the variogram parameters. This disagreement can be attributed to the difference of soil layer thickness. Deeper soil moisture is less to be affected by the external disturbance from land surface.

The numerous SGS realizations gave a description of the possible spatial patterns of soil moisture for each month (Fig. 5), whereas E-type maps depicted the overall variation of soil moisture (Fig. 6). As can be seen from these maps, low soil moisture values concentrated in the sandy deserts and their extensions where eolian sands accumulated due to continuous wind erosion (Liu et al., 2010; Su et al., 2004). Few water sources and strong evaporations facilitated the loss of soil

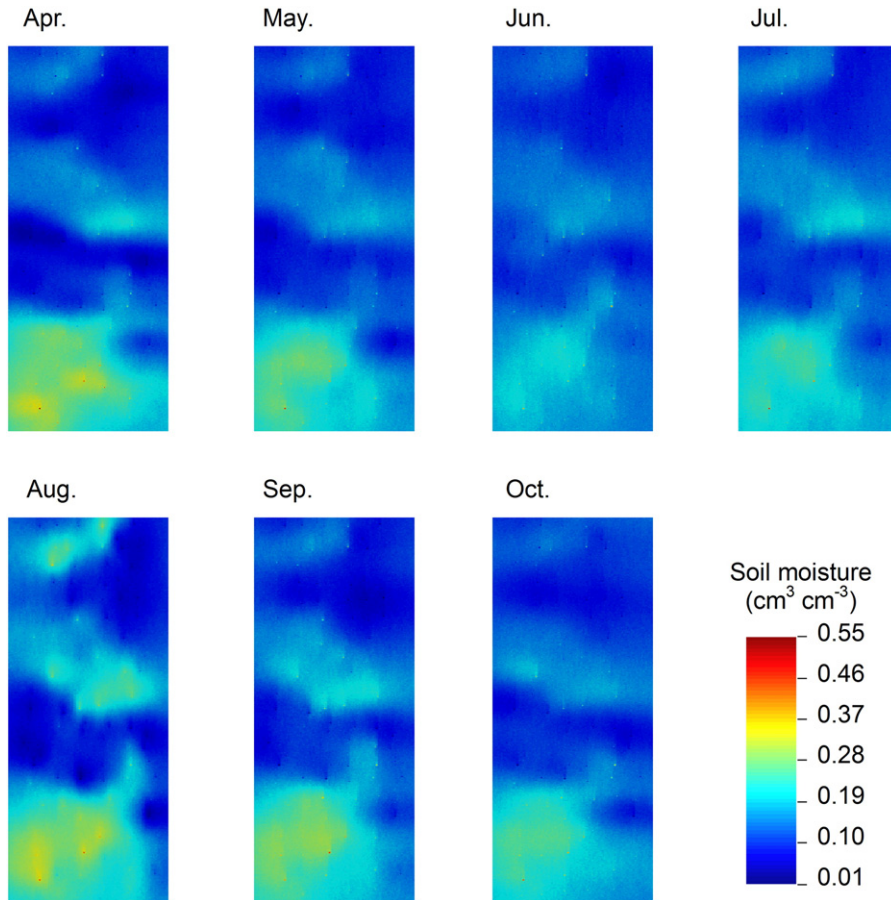


Fig. 6. E-type maps of soil moisture for each month. The E-type values were calculated by averaging the whole set of realizations.

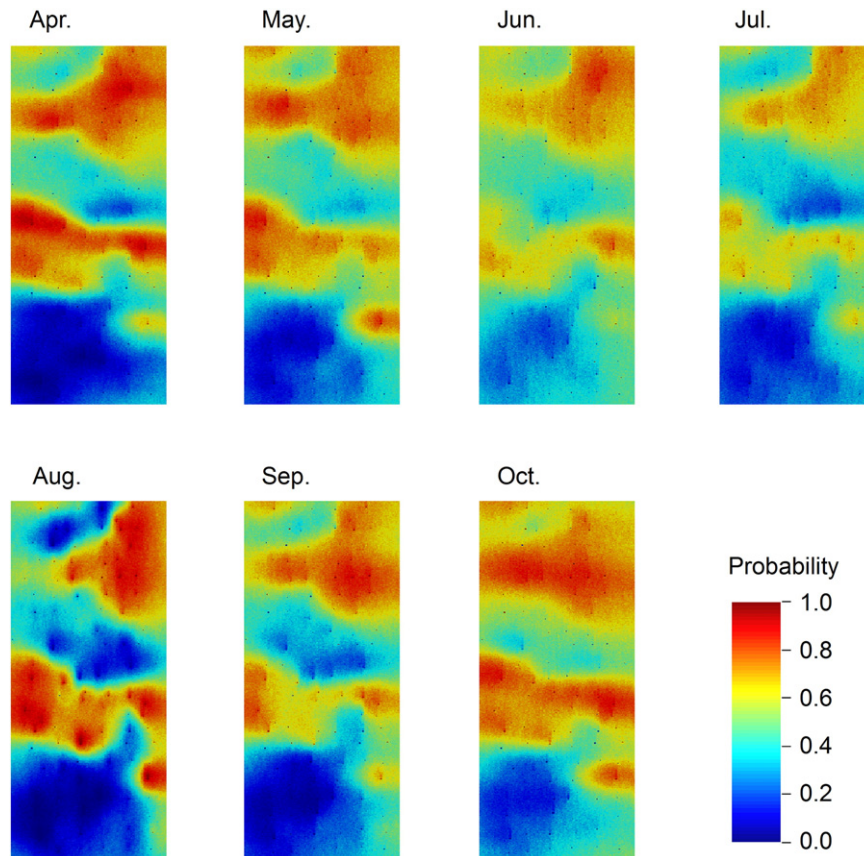


Fig. 7. Probability maps of soil moisture not exceeding $0.15 \text{ cm}^3 \text{ cm}^{-3}$.

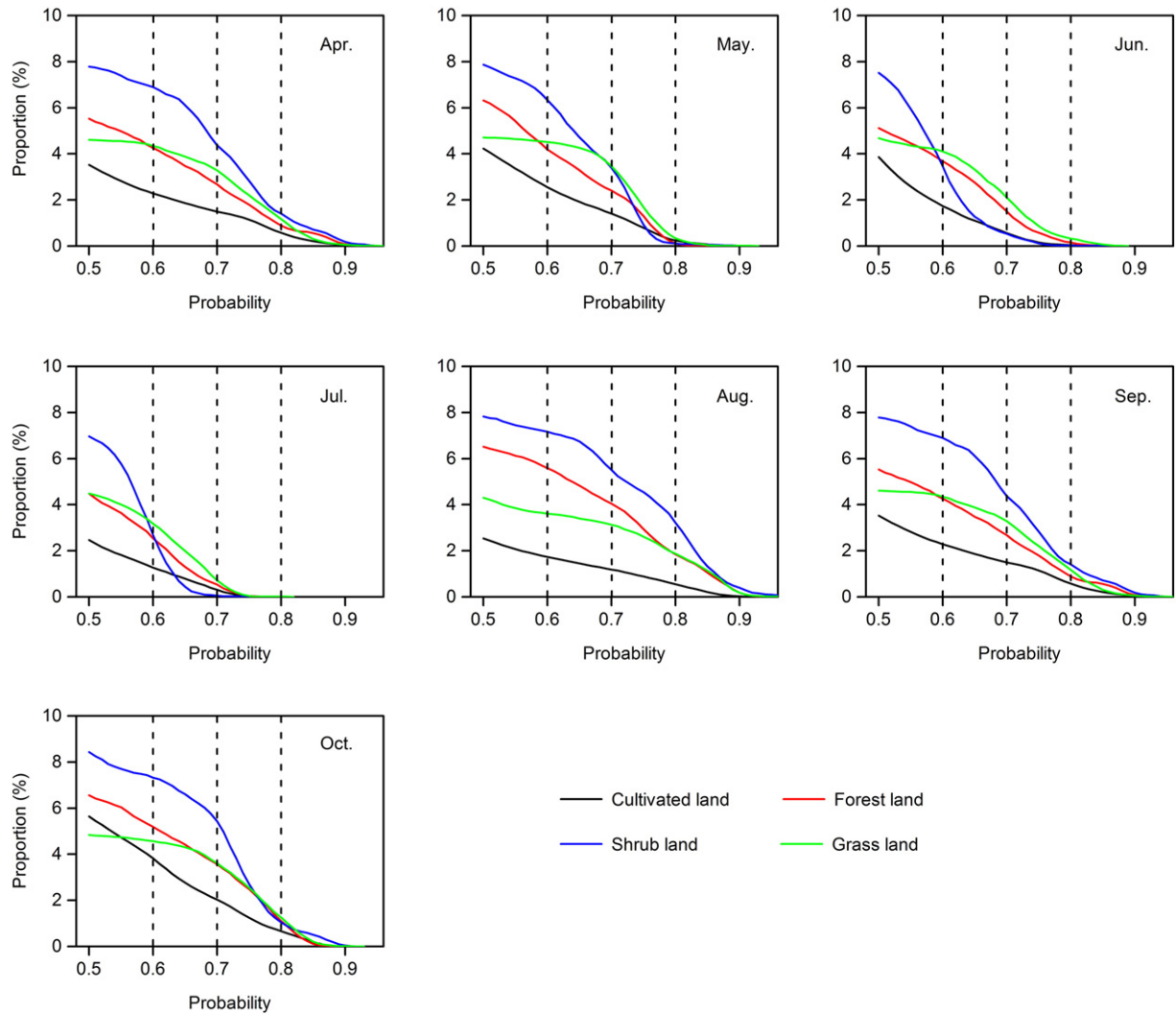


Fig. 8. Proportion of SMS locations in each land use under different spatial probability thresholds.

moisture in these areas. High soil moisture values were mostly located in the cultivated lands because of intermittent irrigation and high water holding capacity of finer-textured soils (Table 1) formed under long-term cultivation (Li and Shao, 2013; Su et al., 2009; Zhao et al., 2010). Moreover, although the stochastic simulation results highlighted spatial variations, the overall spatial patterns of soil moisture from April to October had a certain similarity (Fig. 6). This persistence of spatial patterns over time has often been called temporal stability (Ivanov et al., 2010; Jacobs et al., 2004; Mohanty and Skaggs, 2001; Vachaud et al., 1985). Zhang and Shao (2013) and Li and Shao (2015) found that soil texture, bulk density, soil organic carbon, and vegetation cover were the determinants of the time-stable behaviors in the desert oasis.

4.2. Risk assessment of soil moisture scarcity

The probability of soil moisture not exceeding $0.15 \text{ cm}^3 \text{ cm}^{-3}$ (Fig. 7) provided a measure of the soil moisture uncertainty at a single location. Lower soil moisture locations generally had higher probability values. Based on the probability maps, the locations where SMS existed were easily determined with a given spatial probability threshold of P_s . The SMS areas concentrated in the newly cultivated land and the ecotone of desert and oasis. Choosing the appropriate probability threshold is a subjective decision. By now no unified criterion has been made to identify the critical threshold in literature. In this case, if $P_s > 0.8$, the

SMS areas (Fig. 8) are too small to be managed in practice. So a lower spatial probability such as 0.6 and 0.7 might be more applicable. Delbari et al. (2009) argued that the probability threshold of 0.6 was relatively confidential to delineate vulnerable areas in erosion hazard. If $P_s = 0.6$, 1.3–3.8% of the cultivated land, 2.6–5.2% of the forest land, 3.2–4.6% of the grassland, and 2.7–7.4% of the shrub land were suffering from SMS throughout the growing season. Although the percentages of SMS areas were small, they were key indicators of the eco-environment statement of health.

To prevent land degradation and maintain the sustainability of the agroecosystem, it is imperative to stay on guard against soil moisture scarcity in the oasis. We investigated the irrigation amount in the newly cultivated lands during the study period. The newly cultivated land was irrigated for 9–10 times by conventional flood irrigation with a water quota of approximately 110 mm each time. Generally, the irrigation activities started in early May and ended in early September at the intervals of 12–14 days in the light of soil wetness determined empirically by local farmers. The extensive irrigation restrained the occurrence of widespread SMS at the expense of water resources, but small areas of SMS could not be avoided. Ji et al. (2007) suggested that a higher frequency of irrigation with fewer amounts would be more suitable in this area. Furthermore, forest in the marginal oasis needs to be of concern for the ecological benefit of windbreaks in preventing sands moving toward the fertile land. If possible, the forest land in the oasis margin should be watered. Some protection measures can still be

considered to combat desertification for shrub land and grassland despite the high drought resistance capability of desert plants (Zhao and Cheng, 2002). Controlling the intensity of grazing and curtailing unreasonable land conversion from shrub land and grassland to cultivated land might be wise moves.

5. Conclusions

The spatial variations of soil moisture were analyzed using sequential Gaussian simulation (SGS) with a time series of measurements throughout the growing season in an oasis. Two hundred realizations described the possible spatial distributions of soil moisture for each month. Averaging the overall realizations provided the expected spatial patterns of soil moisture over the study area. We defined soil moisture scarcity (SMS) as a natural event that occurred when the spatial probability of soil moisture not exceeding $0.15 \text{ cm}^3 \text{ cm}^{-3}$ was higher than a critical threshold, and then forecasted the occurrence of SMS under different regulatory probabilities. Spatial analysis showed that SMS locations focused on the newly cleared land and the ecotone of desert and oasis. The proportion of SMS locations in each land use declined at different rates with the increasing of probability thresholds. Considering the values of 0.6 as the critical threshold of spatial probability, 1.3–3.8% of the cultivated land, 2.6–5.2% of the forest land, 3.2–4.6% of the grassland, and 2.7–7.4% of the shrub land were of SMS over the measuring period. To prevent the probable damage to the oasis ecosystem, some protection measures should be considered in the SMS locations during the decision-making processes.

Stochastic simulation is an effective tool to assess the risk of SMS. The prediction of SMS is a stimulus for improving the irrigation efficiency and soil water management in arid regions. The main difficulty issue, however, is to decide on the appropriate probability threshold in practical applications. The utility of outputs using an empirical threshold requires further examination in future studies.

Acknowledgements

The National Natural Science Foundation of China (No. 91025018) provided financial support for this research. Thanks go to the staff members of the Linze Inland River Basin Comprehensive Research Station, Chinese Ecosystem Research Network for their support. We also sincerely appreciate the reviewers and editors for their valuable comments and suggestions.

References

- Afrasiab, P., Delbari, M., 2013. Assessing the risk of soil vulnerability to wind erosion through conditional simulation of soil water content in Sistan plain, Iran. *Environ. Earth Sci.* 70 (6), 2895–2905.
- Berndtsson, R., Nodomi, K., Yasuda, H., Persson, T., Chen, H., Jinno, K., 1996. Soil water and temperature patterns in an arid desert dune sand. *J. Hydrol.* 185 (1), 221–240.
- Bourennane, H., King, D., Couturier, A., Nicoullaud, B., Mary, B., Richard, G., 2007. Uncertainty assessment of soil water content spatial patterns using geostatistical simulations: an empirical comparison of a simulation accounting for single attribute and a simulation accounting for secondary information. *Ecol. Model.* 205 (3), 323–335.
- Cambardella, C., Moorman, T., Parkin, T., Karlen, D., Novak, J., Turco, R., Konopka, A., 1994. Field-scale variability of soil properties in central Iowa soils. *Soil Sci. Soc. Am. J.* 58 (5), 1501–1511.
- Castrignanò, A., Buttafuoco, G., 2004. Geostatistical stochastic simulation of soil water content in a forested area of south Italy. *Biosyst. Eng.* 87 (2), 257–266.
- Chanasyk, D.S., Naeth, M.A., 1988. Measurement of near-surface soil moisture with a hydrogenously shielded neutron probe. *Can. J. Soil Sci.* 68 (1), 171–176.
- Chang, X., Zhao, W., Zeng, F., 2015. Crop evapotranspiration-based irrigation management during the growing season in the arid region of northwestern China. *Environ. Monit. Assess.* 187 (11), 1–15.
- Delbari, M., Afrasiab, P., Loiskandl, W., 2009. Using sequential Gaussian simulation to assess the field-scale spatial uncertainty of soil water content. *Catena* 79 (2), 163–169.
- Deng, J., Chen, X., Du, Z., Zhang, Y., 2011. Soil water simulation and prediction using stochastic models based on LS-SVM for red soil region of China. *Water Resour. Manag.* 25 (11), 2823–2836.
- Deutsch, C.V., Journel, A.G., 1998. *GSLIB: Geostatistical Software Library and User's Guide*. Oxford University Press, New York.
- Duan, X., Xie, Y., Liu, G., Gao, X., Lu, H., 2010. Field capacity in black soil region, Northeast China. *Chin. Geogr. Sci.* 20 (5), 406–413.
- Evett, S.R., Tolk, J.A., Howell, T.A., 2003. A depth control stand for improved accuracy with the neutron probe. *Vadose Zone J.* 2, 642–649.
- Goovaerts, P., 1997. *Geostatistics for Natural Resources Evaluation*. Oxford University Press, New York.
- Goovaerts, P., 1999. Impact of the simulation algorithm, magnitude of ergodic fluctuations and number of realizations on the spaces of uncertainty of flow properties. *Stoch. Env. Res. Risk A.* 13 (3), 161–182.
- Goovaerts, P., 2001. Geostatistical modelling of uncertainty in soil science. *Geoderma* 103 (1), 3–26.
- Hanks, R., Holmes, W., Tanner, C., 1954. Field capacity approximation based on the moisture-transmitting properties of the soil. *Soil Sci. Soc. Am. J.* 18 (3), 252–254.
- Hu, W., Shao, M., Han, F., Reichardt, H., 2011. Spatio-temporal variability behavior of land surface soil water content in shrub- and grass-land. *Geoderma* 162 (3–4), 260–272.
- Ivanov, V.Y., Faticchi, S., Jenerette, G.D., Espeleta, J.F., Troch, P.A., Huxman, T.E., 2010. Hysteresis of soil moisture spatial heterogeneity and the “homogenizing” effect of vegetation. *Water Resour. Res.* 46 (9), W09521.
- Jacobs, J.M., Mohanty, B.P., Hsu, E.-C., Miller, D., 2004. SMEX02: field scale variability, time stability and similarity of soil moisture. *Remote Sens. Environ.* 92 (4), 436–446.
- Ji, X.B., Kang, E.S., Chen, R.S., Zhao, W.Z., Zhang, Z.H., Jin, B.W., 2007. A mathematical model for simulating water balances in cropped sandy soil with conventional flood irrigation applied. *Agric. Water Manag.* 87 (3), 337–346.
- Kairis, O., Kosmas, C., Karavitis, C., Ritsema, C., Salvati, L., et al., 2014. Evaluation and selection of indicators for land degradation and desertification monitoring: types of degradation, causes, and implications for management. *Environ. Manag.* 54 (5), 971–982.
- Lamm, F.R., Rogers, D.H., 2015. The importance of irrigation scheduling for marginal capacity systems growing corn. *Appl. Eng. Agric.* 31 (2), 261–265.
- Leuangthong, O., McLennan, J.A., Deutsch, C.V., 2004. Minimum acceptance criteria for geostatistical realizations. *Nat. Resour. Res.* 13 (3), 131–141.
- Li, D., 2014. *Study on the Spatial and Temporal Variability of Soil Physical Properties in the Middle Basin Oasis of the Heihe River*. (Ph.D. Thesis). Graduate University of Chinese Academy of Sciences (Institute of Soil and Water Conservation, MOE of China), pp. 21–23.
- Li, D., Shao, M., 2013. Simulating the vertical transition of soil textural layers in northwestern China with a Markov chain model. *Soil Res.* 51 (3), 182–192.
- Li, D., Shao, M., 2015. Temporal stability of soil water storage in three landscapes in the middle reaches of the Heihe River, northwestern China. *Environ. Earth Sci.* 73 (7), 3095–3107.
- Li, S., Liang, W., Zhang, W., Liu, Q., 2016. Response of soil moisture to hydro-meteorological variables under different precipitation gradients in the Yellow River Basin. *Water Resour. Manag.* 30 (6), 1867–1884.
- Liu, B., Zhao, W., Chang, X., Li, S., Zhang, Z., Du, M., 2010. Water requirements and stability of oasis ecosystem in arid region, China. *Environ. Earth Sci.* 59 (6), 1235–1244.
- Mohanty, B., Skaggs, T., 2001. Spatio-temporal evolution and time-stable characteristics of soil moisture within remote sensing footprints with varying soil, slope, and vegetation. *Adv. Water Resour.* 24 (9), 1051–1067.
- Pachepsky, Y., Acock, B., 1998. Stochastic imaging of soil parameters to assess variability and uncertainty of crop yield estimates. *Geoderma* 85 (2–3), 213–229.
- Pardo-Iguzquiza, E., Chica-Olmo, M., 2008. Geostatistical simulation when the number of experimental data is small: an alternative paradigm. *Stoch. Env. Res. Risk A.* 22 (3), 325–337.
- Remy, N., Boucher, A., Wu, J., 2009. *Applied Geostatistics with SGeMS: a User's Guide*. Cambridge University Press, New York.
- She, D., Liu, D., Xia, Y., Shao, M., 2014. Modeling effects of land use and vegetation density on soil water dynamics: implications on water resource management. *Water Resour. Manag.* 28 (7), 2063–2076.
- Srivastava, P.K., Han, D., Rico-Ramirez, M.A., Al-Shrafany, D., Islam, T., 2013. Data fusion techniques for improving soil moisture deficit using SMOS satellite and WRF-NOAH land surface model. *Water Resour. Manag.* 27 (15), 5069–5087.
- Stabler, L.B., 2008. Management regimes affect woody plant productivity and water use efficiency in an urban desert ecosystem. *Urban Ecosyst.* 11 (2), 197–211.
- Su, Y.Z., Zhao, H.L., Zhao, W.Z., Zhang, T.H., 2004. Fractal features of soil particle size distribution and the implication for indicating desertification. *Geoderma* 122 (1), 43–49.
- Su, Y.Z., Liu, W.J., Yang, R., Chang, X.X., 2009. Changes in soil aggregate, carbon, and nitrogen storages following the conversion of cropland to alfalfa forage land in the marginal oasis of Northwest China. *Environ. Manag.* 43 (6), 1061–1070.
- Vachaud, G., Passerat de Silans, A., Balabanis, P., Vauclin, M., 1985. Temporal stability of spatially measured soil water probability density function. *Soil Sci. Soc. Am. J.* 49 (4), 822–828.
- Van Meirvenne, M., Goovaerts, P., 2001. Evaluating the probability of exceeding a site-specific soil cadmium contamination threshold. *Geoderma* 102 (1–2), 75–100.
- Vereecken, H., Huisman, J.A., Pachepsky, Y., Montzka, C., van der Kruk, J., Bogena, H., Weiermüller, L., Herbst, M., Martínez, G., Vanderborght, J., 2014. On the spatio-temporal dynamics of soil moisture at the field scale. *J. Hydrol.* 516, 76–96.
- Wang, Y., Xu, X., Lei, J., Li, S., Zhou, Z., Chang, Q., Wang, L., Gu, F., Qiu, Y., Xu, B., 2008. The dynamics variation of soil moisture of shelterbelts along the Tarim Desert Highway. *Chin. Sci. Bull.* 53 (2), 102–108.
- Yan, Q., Zhu, J., Zheng, X., Jin, C., 2015. Causal effects of shelter forests and water factors on desertification control during 2000–2010 at the Horqin Sandy Land region, China. *J. Forest. Res.* 26 (1), 33–45.

- Yao, R.J., Yang, J.S., Shao, H.B., 2013. Accuracy and uncertainty assessment on geostatistical simulation of soil salinity in a coastal farmland using auxiliary variable. *Environ. Monit. Assess.* 185 (6), 5151–5164.
- Zhang, P., Shao, M.a., 2013. Temporal stability of surface soil moisture in a desert area of northwestern China. *J. Hydrol.* 505, 91–101.
- Zhang, Y., Luo, H., Zhang, W., Fan, D., He, Z., Bai, H., 2008. Effects of water deficit on photochemical activity and excitation energy dissipation of photosynthetic apparatus in cotton leaves during flowering and boll-setting stages. *J. Plant Ecol.* 32, 681–689.
- Zhao, W., Cheng, G., 2002. Review of several problems on the study of eco-hydrological processes in arid zones. *Chin. Sci. Bull.* 47 (5), 353–360.
- Zhao, W., Liu, B., 2010. The response of sap flow in shrubs to rainfall pulses in the desert region of China. *Agric. For. Meteorol.* 150 (9), 1297–1306.
- Zhao, W., Liu, B., Zhang, Z., 2010. Water requirements of maize in the middle Heihe River basin, China. *Agric. Water Manag.* 97 (2), 215–223.